Multi-quasiparticle bands in ^{137}Ce

Tumpa Bhattacharjee, Somen Chanda,* Anjali Mukherjee,† Sarmishtha Bhattacharyya, and Swapan Kumar Basu
Variable Energy Cyclotron Centre, Kolkata 700064, India

Sandeep S. Ghugre
UGC-DAE Consortium for Scientific Research, Kolkata 700091, India

U. Dutta Pramanik
Saha Institute of Nuclear Physics, Kolkata 700064, India

R. P. Singh, S. Muralithar, N. Madhavan, J. J. Das, and R. K. Bhowmik
Inter University Accelerator Centre, New Delhi 110067, India
(Received 12 October 2007; published 11 August 2008)

Excited states of ^{137}Ce, populated in the ^{130}Te(^{12}C, 5n) reaction at a beam energy of 65 MeV, have been investigated by $\gamma\gamma$ coincidence spectroscopy using a modest Clover Ge array. Unique spin-parity assignments have been made for most of the levels at high spin and excitation energy by using DCO ratios and polarization information. The known level scheme of ^{137}Ce has been considerably revised on the basis of the new information. A sequence of $M1$ transitions, developed on the 5379.1-keV $\frac{33}{2}\hbar$ level has been suggested to be a positive-parity band through unambiguous assignment of multipolarity of 1124.1- and 836.1-keV γ rays. Another positive-parity bandlike structure has been seen, starting at the 2928.4-keV $\frac{19}{2}^+$ level. Total Routhian surface calculations have been done to predict underlying multi-quasiparticle configurations for the observed bands.

DOI: 10.1103/PhysRevC.78.024304 PACS number(s): 21.10.Re, 23.20.−g, 27.60.+j

I. INTRODUCTION

The transitional nuclei in the light rare-earth region around $A \sim 135$ have been known to exhibit a variety of interesting phenomena [1,2]. Even-even nuclei in this mass region have triaxial deformations that are soft relative to the triaxiality parameter γ [3–5]. The Fermi levels in these nuclei lie in the "prolate-driving" lower $\pi h_{\frac{11}{2}}$ subshell and the "oblate-driving" upper $\nu h_{\frac{11}{2}}$ subshell, respectively. The competing shape-driving effects of the valence protons and neutrons on the γ-soft core is manifested in drastic shape changes with spin and coexistence of different shapes [6,7]. In odd-N nuclei with $N > 74$, low-spin yrast rotational bands built on the $\nu h_{\frac{11}{2}}$ orbital have been seen to exhibit varied amounts of signature splitting, implying nuclear shapes with a significant degree of triaxiality. The experimentally observed signature splittings in the $N = 75, 77$ nuclei, according to the cranked shell model calculations [5,8], imply intermediate values of γ in the collective regime $-60^\circ \leqslant \gamma \leqslant 0^\circ$. An additional feature of the nuclei in this mass region is that they are predicted to show a shallow energy potential with respect to γ. As a consequence, the nuclear shape may stabilize at different values of γ owing to the occupation of various high-j quasiparticles. At higher rotational frequencies, shape changes can be achieved by the rotational alignment of specific quasiparticle pairs [9]. There is increasing evidence for strongly coupled $\Delta I = 1$ bands, built on an oblate ($\gamma = 60^\circ$) multi-particle configuration in odd-N, odd-odd, and even-even nuclei in this mass region, as have been observed in ^{135,136}Ce [10–13], ^{136}La [14], ^{138}Pr [15,16], and ^{138,139}Nd [17,18] recently. The heavier $N \geqslant 77$ nuclei, being less deformed and more γ-soft, are expected to show richer structure dominated by the shape-driving effects of the occupied quasiparticle orbitals. The present study of ^{137}Ce forms part of a systematic study of $N = 79, 80$ nuclei and complements our previous report on ^{136}La [14]. The earlier studies on ^{137}Ce [19–21] used mostly light ions and established a $\pi h^{-2}_{11/2}$ decoupled band structure at low spin [22]. Zhu *et al.* [23] studied the nucleus recently by the ^{124}Sn(^{18}O, 5n)^{137}Ce reaction at 78 MeV and extended the level scheme to $\frac{43}{2}\hbar$. The authors observed a negative-parity oblate band, built on $I = \frac{33}{2}$ with $\gamma \sim -60^\circ$, and suggested a most probable five-quasiparticle (qp) configuration: $\pi g_{\frac{7}{2}} h_{\frac{11}{2}} \otimes \nu s_{\frac{1}{2}} h^2_{\frac{11}{2}}$. However, they could not make definite spin-parity assignments to most of the newly proposed levels, which has been very crucial for the interpretation of the high-spin structure. In the present work, we have attempted to make unambiguous spin-parity assignments by a careful analysis of the directional correlation from oriented states and polarization information and tried to establish a more complete level scheme of ^{137}Ce. A total Routhian surface (TRS) calculation [24–26] with a Woods-Saxon potential and full BCS pairing has been done with a view to interpret the observed band structures.

II. EXPERIMENTAL PROCEDURES AND RESULTS

The excited states of the ^{137}Ce nucleus were populated by using the ^{130}Te(^{12}C, 5n) reaction at 65 MeV at the 15UD

*Corresponding author: somen@veccal.ernet.in; Permanent address: Department of Physics, Fakir Chand College, Diamond Harbour, West Bengal, India.
†Present address: Saha Institute of Nuclear Physics, Kolkata 700064, India.

Pelletron Accelerator of Inter University Accelerator Centre, New Delhi. The target used was of 2.2 mg/cm^2 enriched (99.9%) ^{130}Te, evaporated on a 2.0 mg/cm^2 Au backing, and was created by a 50 μg/cm^2 thin Au film from the top. According to PACE2 calculations [27], the average yield of ^{137}Ce at the center of the target is estimated to be ∼36% of the total reaction cross section whereas the other dominant channel, ^{138}Ce, takes ∼54% share. The experiment was done by using a modest γ array consisting of five Clover Ge detectors, which were placed on two circular rings with the target at the center and making $\pm 18.5^\circ (=\phi)$ with respect to the horizontal plane containing the beam axis (median plane). The positions of the detectors were 81° (for the forward ones) and 138°(for the backward ones), respectively, with respect to the beam direction, when projected on the median plane. The $\gamma\gamma$ coincidence data were acquired in list mode by using the LINUX-based data acquisition software CANDLE [28]. Around 350 million two- and higher fold coincidence events were recorded. The pulse height of each segment of the Clover detectors was gain matched to 0.5-keV/channel and the "add-back" spectra were generated by following the standard procedure [29]. The raw list data were sorted to generate several 4096 × 4096 total $E_\gamma - E_\gamma$ matrices by using the computer code INGASORT [30] and the gated coincidence spectra were projected to extract the coincidence information. The γ rays belonging to ^{137}Ce were identified by putting gates on strong known transitions [22,23] and by excluding the γ rays belonging to ^{138}Ce [31,32]. Figures 1 and 2 show a few added coincidence spectra of interest, corresponding to the transitions that have been assigned to different bandlike sequences in the proposed level scheme of ^{137}Ce (cf. Fig. 4).

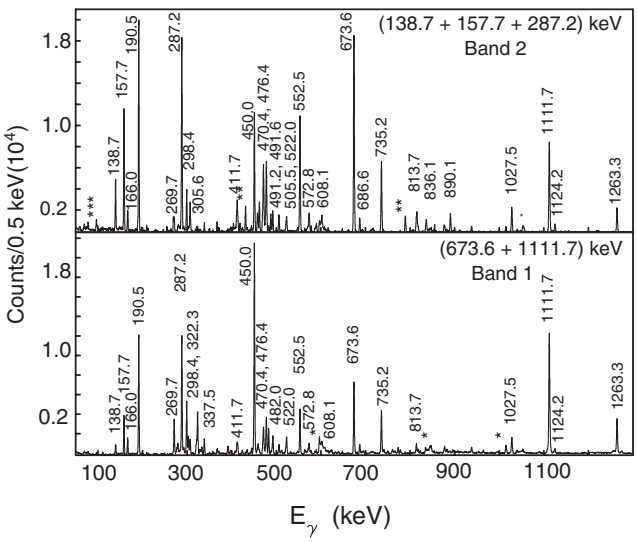

FIG. 1. Representative coincidence spectra corresponding to the added gates of interest as indicated, belonging to the ^{137}Ce nucleus, for band 1 and band 2 as obtained from $\gamma\gamma$ matrix analysis. The peaks marked as $*$ are coming from random coincidence with commonly known background lines; the peaks marked as $**$ are coming from random coincidences with the γ lines from the isomeric levels of the other populated Ce nuclei, and the peaks marked as $***$ could not be placed.

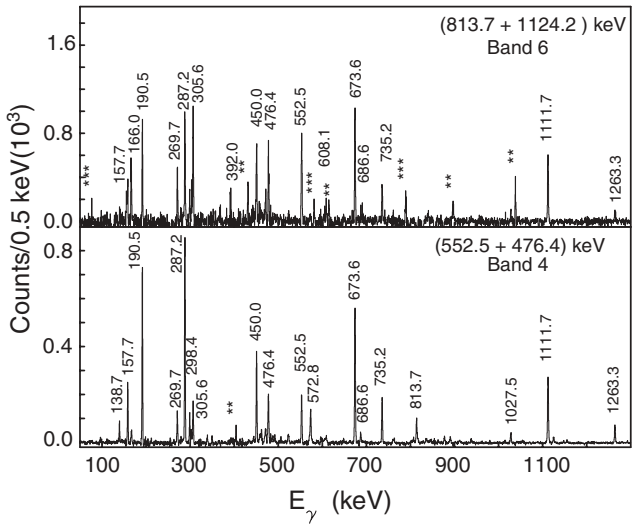

FIG. 2. Representative coincidence spectra corresponding to the added gates of interest as indicated, belonging to ^{137}Ce nucleus, for band 4 and band 6 as obtained from $\gamma\gamma$ matrix analysis. The peaks marked as $*$ are coming from random coincidence with commonly known background lines; the peaks marked as $**$ are coming from random coincidences with the γ lines from the isomeric levels of the other populated Ce nuclei, and the peaks marked as $***$ could not be placed.

These, along with the similar spectra, have been used in the construction of a consistent level scheme of ^{137}Ce.

The multipolarities of the observed transitions were determined by using the directional correlation from oriented states (DCO) ratio method following the prescriptions of Krämer-Flecken *et al.* [33]. For this, another 4096 × 4096 matrix was generated with the events detected in the 81° Clovers along the x-axis and the corresponding events detected in coincidence in the 138° Clovers along the y-axis. The deduced DCO ratios for most of the γ rays have been obtained against the 673.6-keV ($\frac{15}{2}^- \rightarrow \frac{11}{2}^-$) known $E2$ gate. Typical values for the extracted DCO ratio come out to be 1.0 for pure quadrupole transitions and 0.6 for pure dipole transitions in the present analysis, which are corroborated by the analysis of known $E2$ and $M1$ transitions in ^{137}Ce and ^{138}Ce nuclei, respectively. For the weak transitions from higher spin states, the ratios were cross-checked by adding the gated spectra of the same multipolarity in the cascade.

To infer the parity of the levels, especially for the levels connected by the dipole transitions, we have deduced the polarization directional correlation asymmetry parameter ($\Delta_{\rm PDCO}$) of the transitions from the coincidence list data following Refs. [34–36]. As is well known, the polarization effect is maximum at 90° with respect to the beam direction. The Clovers sitting at 81° were used for this purpose as there is no detector sitting at 90°. The $\Delta_{\rm PDCO}$ has been extracted by using the spectra recorded by these detectors, gated by the γ rays detected at 138°. It may be mentioned that according to Droste *et al.* [35], the sign of the polarization asymmetry remains unaltered for a particular multipolarity, as long as the ϕ angle, following the convention used in Ref. [35], is less than 90°. Therefore, we have taken those detector pairs

in the polarization analysis for which $\phi < 90^\circ$. Accordingly, the asymmetry parameter $\Delta_{\rm PDCO}$ was obtained by using the relation

$$\Delta_{\rm PDCO} = \frac{a(E_\gamma)N_\perp - N_\parallel}{a(E_\gamma)N_\perp + N_\parallel}, \quad (1)$$

where $N_\parallel$ and $N_\perp$ are the counts for the actual Compton scattered γ rays in the planes parallel and perpendicular to the reaction plane in the 81° Clovers, which reflect the extent of polarization in a typical situation. The correction from asymmetry in the response of the Clover segments, as defined by $a(E_\gamma) = \frac{N_\parallel}{N_\perp}$, was checked by using a ^{152}Eu source and was found to be close to unity, as expected. By using the fitted parameter $a(E_\gamma)$, $\Delta_{\rm PDCO}$ for most of the γ rays in ^{137}Ce have been determined. A positive value of $\Delta_{\rm PDCO}$ means that the transition is electric whereas a negative value favors a magnetic transition. Since the angular correlation effects between the 81° and 138° detectors are similar for both of parallel and perpendicular scattering, the effects get nullified in Eq. (1). Moreover, in this qualitative analysis we are interested more in the sign of $\Delta_{\rm PDCO}$ than its magnitude. As the nuclei ^{138,139}Ce were also produced in the same reaction along with ^{137}Ce, the deduced $\Delta_{\rm PDCO}$ values for a few known transitions from these nuclei (e.g., 0.06 ± 0.03 for the 673.6-keV $E2$ transition in ^{137}Ce, 0.04 ± 0.03 for the 788.6-keV $E2$ transition in ^{138}Ce, and 0.08 ± 0.04 for the 270.7-keV $E2$ transition in ^{139}Ce) could reproduce the electric nature of these transitions. This shows the reliability of the present analysis. Figure 3 shows the polarization spectra for some of the transitions of interest in which the spectra of

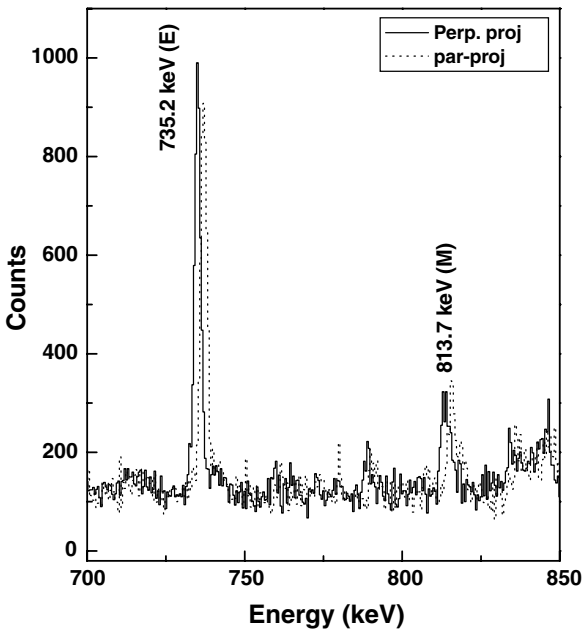

FIG. 3. Polarization spectra for the 735.2-keV ($\frac{23}{2}^+ \rightarrow \frac{21}{2}^-$) and 813.7-keV ($\frac{35}{2}^+ \rightarrow \frac{33}{2}^+$) transitions in coincidence with the 673.6-keV ($\frac{15}{2}^- \rightarrow \frac{11}{2}^-$) transition. The spectra of γ rays, scattered in the direction perpendicular and parallel to the emission plane, are shown by solid and dotted lines, respectively. An offset of 2.0 keV has been introduced between the two spectra to guide the eye.

γ rays, scattered in the directions perpendicular and parallel to the reaction plane, are shown by solid and dashed lines, respectively. The comparison clearly shows that the 813.7-keV dipole transition is magnetic, whereas the 735.2-keV dipole transition is electric in character. These findings have been very crucial in fixing the spin-parity of the higher spin states above 2.5 MeV. The $\Delta_{\rm PDCO}$ values showing a definite sign (positive or negative) have been indicated in Table I against the corresponding transitions. The values quoted in the table have been obtained, in most cases, from the 673.6-keV gate and those for the 673.6-keV transition are from the 1112.7-keV gate. For the weaker transitions, where the statistics is low, we have added the gates of a few transitions in the cascade. As already indicated, the DCO results in conjunction with the polarization correlation information have been used to make definite spin-parity assignments to most of the higher spin levels in ^{137}Ce, which was not possible in the previous work of Zhu *et al.* [23].

III. CONSTRUCTION OF THE LEVEL SCHEME OF ^{137}Ce

The level scheme of ^{137}Ce, as deduced from the present study, is shown in Fig. 4. The placement of the γ transitions in the scheme is based on the $\gamma\gamma$ coincidence relationships and their relative intensities along with the available or adopted experimental results from earlier experiments [22,23]. The spin-parity assignments of the levels, in particular, the higher spin members, have been made on the basis of the deduced DCO ratios and the polarization asymmetry information, as described in the previous section. The results, extracted from the present work, are consistent with those of earlier work [22] and supersede the work of Zhu *et al.* [23] with respect to more definite spin-parity assignments to the higher lying bandlike sequences. The energies and the relative intensities of the assigned γ rays, together with other relevant information concerning their placement in the level scheme, are given in Table I. Because of the presence of overlapping γ rays from ^{138,139}Ce, the relative intensities, in some cases, were either obtained from the analysis of the appropriate gated spectra or checked for consistency from the gated spectra of specific transitions. Six bandlike sequences, as labeled in Fig. 4, have been identified. Of these, band 2 and band 6 will be discussed in detail, as it was possible to make unique spin-parity assignments for the members of these sequences, which were only tentatively done in the work of Zhu *et al.* [23].

Band 1 is built on the $34.4\,h$, $11/2^-$ isomeric state at 254.3 keV and continues up to the $\frac{27}{2}^-$ state at 3694.0 keV, connected by relatively weaker transitions beyond $\frac{21}{2}^-$. This band connects to band 2 at 3224.8 keV ($\frac{23}{2}^+$) by the 735.2-keV γ ray that was tentatively assigned as $E1$ multipolarity from the DCO analysis by Zhu *et al.* [23]. In this work, we have made a firm assignment of $E1$ multipolarity to the 735.2-keV γ ray from DCO and polarization asymmetry analysis. This has resulted in definite parity assignments to the sequence, labeled as band 2, which starts at 2928.4 keV ($\frac{19}{2}^+$). This band extends up to the ($\frac{31}{2}^+$) level at 4703.6 keV by a cascade of mixed transitions and has been conjectured to be a three-qp band (cf. next section).

TABLE I. List of γ rays belonging to ^{137}Ce, as observed in the present work along with their assignments.

E_γ[a] (in keV)	$J_i^\pi \rightarrow J_f^\pi$	I_γ[b]	$R_{\rm DCO}$ (Err)	$\Delta_{\rm PDCO}$[c] (Err)	Deduced multipolarity
48.6[d]	$19/2^- \rightarrow 21/2^-$	2.5	–	–	$M1+E2$
49.8[d]	$27/2^+ \rightarrow 25/2^-$	0.5	–	–	$(E1+M2)$
96.4	$23/2^+ \rightarrow 21/2^+$	1.3	1.48(0.5)	–	$M1+E2$
138.7	$21/2^+ \rightarrow 19/2^+$	2.2	0.9(0.15)	–	$M1+E2$
157.7	$23/2^+ \rightarrow 21/2^+$	5.5	0.86(0.04)	–	$M1+E2$
165.7[d]	$(27/2^+) \rightarrow 25/2^+$	4.1	–	–	$M1+E2$
166.0	$35/2^+ \rightarrow 33/2^+$	4.2	1.17(0.15)[e]	–	$M1+E2$
172.6	$25/2^- \rightarrow 23/2^-$	0.5	0.91(0.28)[f]	–	$(M1+E2)$
190.5	$25/2^+ \rightarrow 23/2^+$	15.6	0.75(0.01)	–	$M1+E2$
192.0	$25/2^- \rightarrow 23/2^+$	1.3	–	–	$(M1+E2)$[g]
254.3	$11/2^- \rightarrow 3/2^+$	–	–	–	$M4$[h]
267.9	$17/2^+ \rightarrow 17/2^+$	1.0	–	–	$M1+E2$[g]
269.7	$31/2^+ \rightarrow 27/2^+$	4.9	1.07(0.06)	0.24(0.12)	$E2$
276.2	$23/2^+ \rightarrow 21/2^+$	1.1	0.79(0.26)	–	$(M1+E2)$
279.3	$25/2^+ \rightarrow 23/2^+$	3.2	0.73(0.14)	–	$M1+E2$
287.2	$27/2^+ \rightarrow 25/2^+$	19.4	0.65(0.01)	−0.04(0.03)	$M1$
298.4	$21/2^- \rightarrow 19/2^-$	11.7	1.4(0.05)	–	$M1+E2$
301.4	$27/2^+ \rightarrow 25/2^+$	2.6	0.59(0.07)	–	$M1+E2$
305.6	$37/2^+ \rightarrow 35/2^+$	2.1	0.57(0.08)	–	$M1+E2$
320.1	$25/2^+ \rightarrow 23/2^+$	1.9	0.61(0.09)	−0.17(0.09)	$M1$
322.3	$23/2^- \rightarrow 21/2^-$	7.0	0.63(0.04)	–	$M1+E2$
337.5	$23/2^+ \rightarrow 21/2^+$	3.2	0.45(0.05)	–	$M1+E2$
349.0	$(39/2^+) \rightarrow (37/2^+)$	0.8	0.43(0.14)[i]	–	$(M1+E2)$
366.8	$19/2^+ \rightarrow 21/2^+$	0.9	0.98(0.37)[j]	–	$(M1+E2)$
370.4	$21/2^+ \rightarrow 19/2^-$	0.6	1.16(0.26)[k]	–	$(E1+M2)$
390.5	$27/2^- \rightarrow 25/2^-$	1.2	0.67(0.14)	–	$(M1+E2)$
411.7	$29/2^+ \rightarrow 27/2^+$	6.3	1.13(0.13)[i]	–	$M1+E2$
443.7	$25/2^+ \rightarrow 23/2^-$	0.9	1.04(0.28)[f]	–	$(E1+M2)$
450.0	$21/2^- \rightarrow 19/2^-$	41.1	0.56(0.007)	−0.04(0.03)	$M1$
456.7	$17/2^+ \rightarrow 15/2^-$	3.4	–	–	$(E1+M2)$[g]
459.1	$25/2^+ \rightarrow 23/2^+$	3.4	0.67(0.14)	–	$M1+E2$
461.5	$19/2^+ \rightarrow 17/2^+$	3.2	0.55(0.3)[j]	–	$(M1+E2)$[g]
470.4	$39/2^+ \rightarrow 37/2^+$	6.1	0.56(0.05)	−0.10(0.08)	$M1$
476.4	$33/2^+ \rightarrow 31/2^+$	8.7	0.98(0.11)[f]	–	$M1+E2$
482.0	$23/2^- \rightarrow 21/2^-$	3.5	0.51(0.03)	−0.17(0.15)	$M1$
486.4	$17/2^+ \rightarrow 15/2^-$	2.3	–	–	$(E1+M2)$[g]
491.2	$19/2^+ \rightarrow 17/2^+$	1.2	0.77(0.12)[f]	–	$(M1+E2)$[g]
491.6	$25/2^- \rightarrow 23/2^-$	4.4	0.49(0.11)	–	$M1+E2$
505.5	$21/2^+ \rightarrow 21/2^+$	2.5	0.66(0.1)	–	$(M1+E2)$
522.0	$21/2^+ \rightarrow 19/2^-$	5.2	1.26(0.2)	–	$E1+M2$
552.5	$31/2^+ \rightarrow 27/2^+$	10.9	1.10(0.04)	0.12(0.04)	$E2$
572.8	$35/2^+ \rightarrow 33/2^+$	2.7	0.41(0.05)[f]	–	$M1+E2$
589.4	$31/2^+ \rightarrow 29/2^+$	2.2	–	–	$(M1+E2)$[g]
608.1	$(41/2^+) \rightarrow 39/2^+$	0.4	–	–	$(M1+E2)$[h]
673.6	$15/2^- \rightarrow 11/2^-$	94.0	1.6(0.02)[f]	0.06(0.03)	$E2$
681.8	$27/2^+ \rightarrow 25/2^-$	0.9	0.95(0.44)	–	$(E1+M2)$
686.6	$23/2^+ \rightarrow 19/2^-$	3.4	1.0(0.1)	−0.23(0.14)	M2
731.1	$(43/2^+) \rightarrow (41/2^+)$	≤ 0.1	–	–	$(M1+E2)$[h]
735.2	$23/2^+ \rightarrow 21/2^-$	18.5	0.57(0.02)	0.08(0.06)	$E1$
760.5[k]	$27/2^+ \rightarrow 23/2^+$	1.7	0.79(0.22)	–	$(E2)$
772.3	$23/2^- \rightarrow 19/2^-$	1.3	0.74(0.13)	–	$(E2)$
777.6	$(29/2^+) \rightarrow (27/2^+)$	0.4	0.87(0.25)	–	$(M1+E2)$
805.8	$(37/2^+) \rightarrow 35/2^+$	0.4	1.06(0.3)	–	$(M1+E2)$
813.7	$35/2^+ \rightarrow 33/2^+$	5.3	1.0(0.09)[l]	−0.16(0.12)	$M1$
836.1[d]	$15/2^- \rightarrow 13/2^-$	2.3	–	–	$(M1+E2)$

TABLE I. *(Continued.)*

E_γ[a] (in keV)	$J_i^\pi \rightarrow J_f^\pi$	I_γ[b]	R_{DCO} (Err)	Δ_{PDCO}[c] (Err)	Deduced multipolarity
875.9	$21/2^+ \rightarrow 19/2^-$	2.7	0.39(0.11)	–	$(E1+M2)$
882.1	$27/2^- \rightarrow 23/2^-$	1.5	0.30(0.15)	–	$(E2)$
890.1	$13/2^- \rightarrow 11/2^-$	4.8	–	–	$M1+E2$[h]
937.2	$21/2^+ \rightarrow 19/2^-$	2.6	0.53(0.09)	0.16(0.14)	$E1$
963.9[k]	$25/2^- \rightarrow 23/2^-$	1.3	0.66(0.21)	–	$(M1+E2)$[g]
1027.5	$21/2^+ \rightarrow 19/2^-$	7.0	0.58(0.04)	0.12(0.07)	$E1$
1052.6[d]	$15/2^- \rightarrow 15/2^-$	1.8	0.74(0.25)	–	$(M1+E2)$
1054.6	$17/2^+ \rightarrow 13/2^-$	0.9	–	–	$(M1+E2)$[g]
1111.7	$19/2^- \rightarrow 15/2^-$	67.0	1.6(0.02)[f]	0.11(0.02)	$E2$
1124.1	$33/2^+ \rightarrow 31/2^+$	3.2	1.2(0.2)[e]	–	$M1+E2$
1154.8[d]	$(39/2^+) \rightarrow 35/2^+$	0.6	–	–	$(E2)$
1253.9	$23/2^+ \rightarrow 21/2^-$	0.5	1.14(0.44)[f]	–	$(M1+E2)$[g]
1263.3	$19/2^- \rightarrow 15/2^-$	20.2	0.85(0.03)	0.06(0.05)	$E2$
1273.3	$23/2^- \rightarrow 21/2^-$	1.9	0.63(0.15)[f]	–	$M1+E2$
1445.9[d]	$25/2^- \rightarrow 21/2^-$	1.9	1.5(0.35)	–	$(E2)$
1509.3	$17/2^+ \rightarrow 15/2^-$	0.6	–	–	$(E1+M2)$[g]
1726.2	$15/2^- \rightarrow 11/2^-$	1.1	–	–	$E2$

[a]Typical uncertainty in energy is ±0.1–0.2 keV.
[b]Relative γ-ray intensities are estimated from prompt spectra and normalized to 100 for the total intensity of 673.6-, 890.1-, and 1726.2-keV γ rays. Overall uncertainty from peak fitting and efficiency calibration is estimated to be of the order of 10% for strong transitions and 15%–20% for weak transitions.
[c]Only conclusive values have been given. For the rest, the PDCO ratio is inconclusive.
[d]Transitions not observed; value adopted from coincidence and intensity considerations.
[e]From the 287.2-keV ($M1$) DCO gate.
[f]From the 450.0-keV ($M1$) DCO gate.
[g]Adopted in the present work.
[h]Adopted from previous work [22].
[i]From the 673.6-keV ($E2$) DCO gate.
[j]From the 1263.3.0-keV ($E2$) DCO gate.
[k]Placed in the present work.
[l]From the 450.0 + 735.2 + 287.2 keV (all $M1$) sum DCO gate.

Band 2 is linked to band 4 and band 6 by a 552.5-keV γ ray of $E2$ multipolarity, at the 3702.5-keV ($\frac{27}{2}^+$) level, as suggested by Zhu *et al.* [23], which is corroborated by the present work. Band 4 starts from $\frac{31}{2}^+$ at the 4225.0-keV level and extends to the ($\frac{39}{2}^+$) level at 6459.0 keV. The other links to the sequence, labeled as band 6, are the 1124.1-keV transition to the 5379.1-keV level and the 813.7-keV transition to the 5545.1-keV level, respectively. Incidentally, both the 813.7- and 1124.1-keV γ rays were tentatively assigned to be of $E1$ multipolarity by Zhu *et al.* [23], which resulted in $\frac{33}{2}^-$ and $\frac{35}{2}^-$ spin-parity assignments to the levels at 5379.1 and 5545.1 keV, respectively. In the present work, we have definitely confirmed that the 813.7-keV γ ray has $M1$ multipolarity whereas, the 1124.1-keV γ ray turns out to be of $M1+E2$ multipolarity from the DCO ratio and polarization asymmetry information. Based on these, we have assigned positive parity to the sequence, labeled as band 6, in contrast to the assignment of Zhu *et al.* [23]. The other nonyrast low-lying levels and sequences, labeled as band 3 and band 5, have been retained following Zhu *et al.* [23] and have been corroborated by our coincidence data.

IV. DISCUSSION

The level structure of ^{137}Ce, as depicted in Fig. 4, shows a very complex character at low and moderate excitation energy and spin, typical of a near-spherical nucleus. Bandlike sequences are seen above the 2.5-MeV excitation, which need to be examined in the light of our present understanding of this nucleus and the neighboring Ce nuclei. To characterize the rotational properties of bands 2 and 6, the experimental alignments have been plotted in Fig. 5 as a function of rotational frequency. The alignment is defined, following Bengtsson and Frauendorf [37], as

$$i_x(\omega) = I_x(\omega) - I_{x,\mathrm{ref}}(\omega), \tag{2}$$

where I_x is estimated as $I_x = [(I+\frac{1}{2})^2 - \langle K\rangle^2]^{\frac{1}{2}}$ and $I_{x,\mathrm{ref}}$ is based on a frequency-dependent reference moment of inertia, given by $\Im_{\mathrm{ref}} = \Im_0 + \omega^2\Im_1$. The values of the Harris parameters [30]$\Im_0$ and $\Im_1$, for the reference moment of inertia, have been obtained by fitting linearly the $\frac{E(I)}{I(I+1)}$ versus ω^2 data for the ground-state band and have been found to be very similar to those obtained for ^{135}Ce (e.g., $\Im_0 = 3.5$ and $\Im_1 = 34.7$ [10]). The value of $\langle K\rangle$ for each band is set equal

FIG. 4. Level scheme of the ^{137}Ce nucleus, as proposed in the present work. For details, see the text.

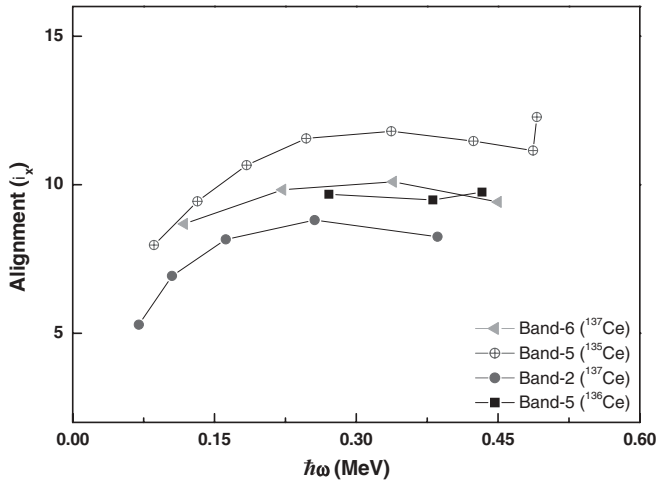

FIG. 5. Experimental alignments for band 2 and band 6 of ^{137}Ce shown as a function of rotational frequency. The experimental alignments for the bands from neighboring nuclei have been shown for comparison. See text for details.

to the angular momentum of the bandhead. In the cases where the angular momentum of the lowest observed state in a band is not given by the K value, we use the value of K obtained from a fit of the level energies as a quadratic function of spin I. In our case, fractional values were obtained for K and the nearest half-integer value has been adopted. The experimental Routhian is determined, following Ref. [37], from the expression

$$E'(I) = \tfrac{1}{2}[E(I+1) + E(I-1)] - \omega(I) I_x(I), \qquad (3)$$

where the average value of $E(I+1)$ and $E(I-1)$ is used as an approximation for $E(I)$. Since we are interested in the differences between the Routhians $E'(I)$ in a band, the correction coming from the reference configuration cancels out. Therefore, we do not attempt any correction from the reference configuration. In Figs. 9 and 10 the experimental and theoretical Routhians for bands 2 and 6, respectively, have been plotted and compared. Table II summarizes the proposed quasiparticle structures associated with the bands.

TABLE II. Proposed quasiparticle structure of the bands in ^{137}Ce.

Band 2	$\nu[h_{\frac{11}{2}}]^2 \otimes \nu[s_{\frac{1}{2}}]$ and $\pi[g_{\frac{7}{2}} h_{\frac{11}{2}}] \otimes \nu[h_{\frac{11}{2}}]$ above $\frac{25}{2}\hbar$
Band 3	$\pi[g_{\frac{7}{2}} d_{\frac{5}{2}}] \otimes \nu[s_{\frac{1}{2}}]$
Band 4	$\pi[g_{\frac{7}{2}} d_{\frac{5}{2}} h^2_{\frac{11}{2}}] \otimes \nu[s_{\frac{1}{2}}]$
Band 6	$\pi[g_{\frac{7}{2}} h_{\frac{11}{2}}] \otimes \nu[h_{\frac{11}{2}} g^2_{\frac{7}{2}}]$

A. Band 1

The negative-parity ground-state band (band 1) is developed above the $\frac{11}{2}^-$ state at 254.3 keV and is associated with the unique parity high-j orbital $\nu h_{\frac{11}{2}}$. This band extends up to the $\frac{27}{2}^-$ state at 3694.0 keV; however, the major intensity is taken over by a positive-parity sequence (band 2), which connects band 1 by a 735.2-keV $E1$ transition to the 2489.6-keV ($\frac{21}{2}^-$) level. According to the earlier work [21], the ground-state band is triaxial in nature with $\gamma \sim -30^\circ$, midway between the prolate ($\gamma = 0^\circ$, $\Omega = \frac{11}{2}$) and the oblate ($\gamma = -60^\circ$, $\Omega = \frac{11}{2}$) shape.

B. Band 2

This band was assigned tentatively to be a positive-parity band by Zhu *et al.* [23] and has been confirmed in our work by a definite assignment of $E1$ multipolarity to the 735.2-keV transition. The band actually starts at the $\frac{19}{2}^+$ (2928.4-keV) level; however, the lower members of this band are weakly populated because of the 735.2-keV transition, which is reducing the major intensity. The lower members of this band connect to the nonyrast levels, eventually leading to the $\frac{19}{2}^-$ level at 2039.6 keV. In Fig. 6, the theoretical DCO ratios have been plotted for the 287.2- and 190.5-keV transitions with respect to the 552.5-keV transition for different mixing ratios and have been compared with the corresponding experimental DCO ratios. The comparison shows that the 287.2- and 190.5-keV γ rays are indeed pure $M1$ transitions with the $E2/M1$ mixing ratio very close to zero. As the bandhead energy is around 2.5 MeV lower than that of band 6,

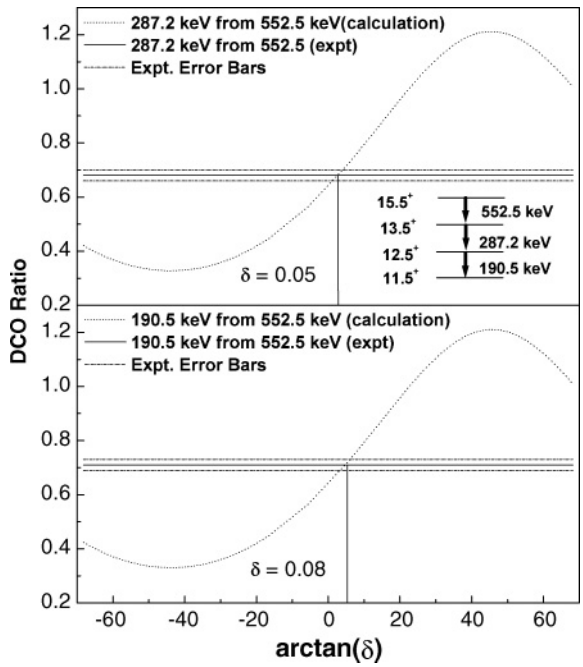

FIG. 6. The experimental DCO ratio for the 287.2- and 190.5-keV transitions with respect to the 552.5-keV $E2$ transition, compared with the theoretical DCO values.

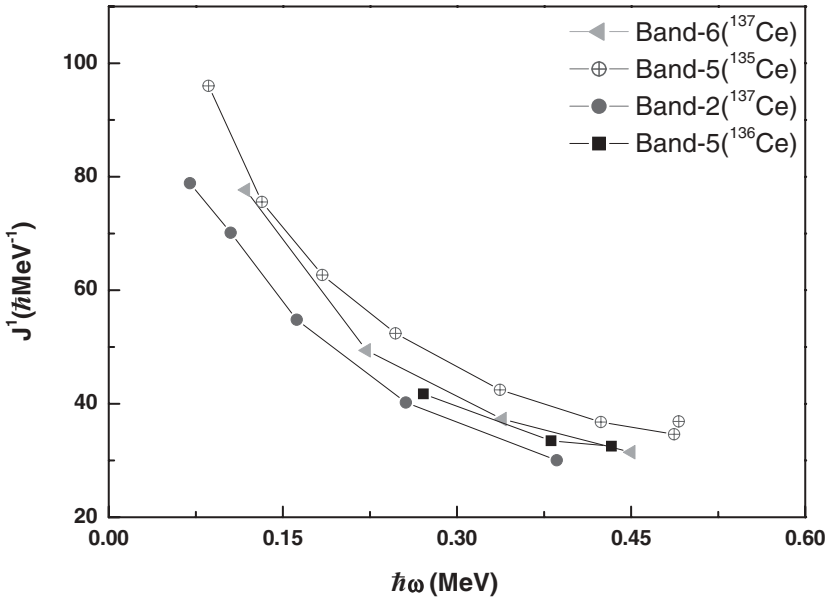

FIG. 7. Kinematic moments of inertia ($J^{(1)}$) for band 2 and band 6 of ^{137}Ce shown as a function of rotational frequency. The experimental values corresponding to the bands from neighboring nuclei have been shown for comparison. See text for details.

which is most likely a five-qp band, as suggested by earlier workers [23], a three-qp configuration appears to be quite appropriate for band 2. Assuming the bandhead spin to be $\frac{19}{2}\hbar$, we have calculated the alignment (i_x), kinematic moment of inertia ($J^{(1)}$), and dynamic moment of inertia ($J^{(2)}$) for band 2 from the experimental data and plotted these against the rotational frequency ω in Figs. 5, 7, and 8, respectively, along with the same quantities for band 6. The alignment of this band has been found to be less than that of band 6. The lower values of i_x and $J^{(2)}$ for band 2 suggest the involvement of fewer quasiparticles and a plausible oblate character. We have performed the TRS calculation [24–26] for this band with different three-qp configurations for the bandhead. The choice of plausible configurations is guided by the suggested configurations for band 1 and band 2 in ^{135}Ce [10], appearing around similar excitation energy as the present band. Of these two bands of ^{135}Ce, band 1 is a positive-parity $M1$ band with $E2$ crossover transitions and it has been conjectured to have a likely three-qp configuration [$\pi g_{\frac{7}{2}} h_{\frac{11}{2}} \otimes \nu h_{\frac{11}{2}}$ (Conf1)] by Ma *et al.* [10]. Band 2 of ^{135}Ce, in contrast, is suggested to be a positive-parity $E2$ band [10], having an associated three-neutron quasiparticle configuration [i.e., $\nu h^2_{\frac{11}{2}} \otimes \nu s_{\frac{1}{2}}$ (Conf2)], which is oblate in shape ($\gamma \sim -60^\circ$). In Fig. 9, the theoretical Routhians for band 2 of ^{137}Ce have been plotted against ω for the two configurations (Conf1 and Conf2) and these have been compared with the corresponding experimental Routhians. It is observed that the theoretical curves for Conf1 and Conf2 are parallel to those obtained from the experimental data and both of these show minima around $\gamma \sim -90^\circ$. However, the minima for Conf1 becomes stable only above a frequency 0.3 MeV, corresponding to $\sim\frac{25}{2}\hbar$ in spin. In contrast, Conf2 cannot explain the highest spin states populated in the

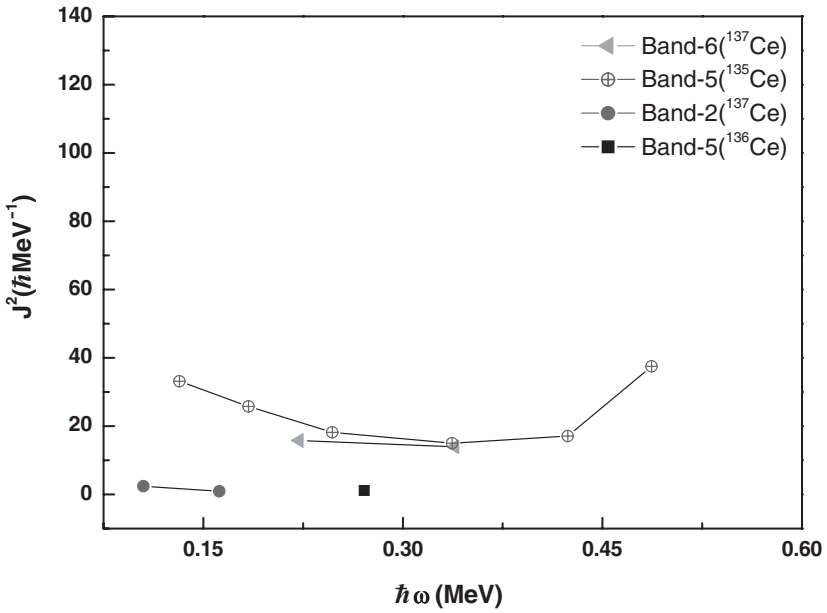

FIG. 8. Dynamic moments of inertia ($J^{(2)}$) for band 2 and band 6 of ^{137}Ce shown as a function of rotational frequency. The experimental values corresponding to the bands from neighboring nuclei have been shown for comparison. See text for details.

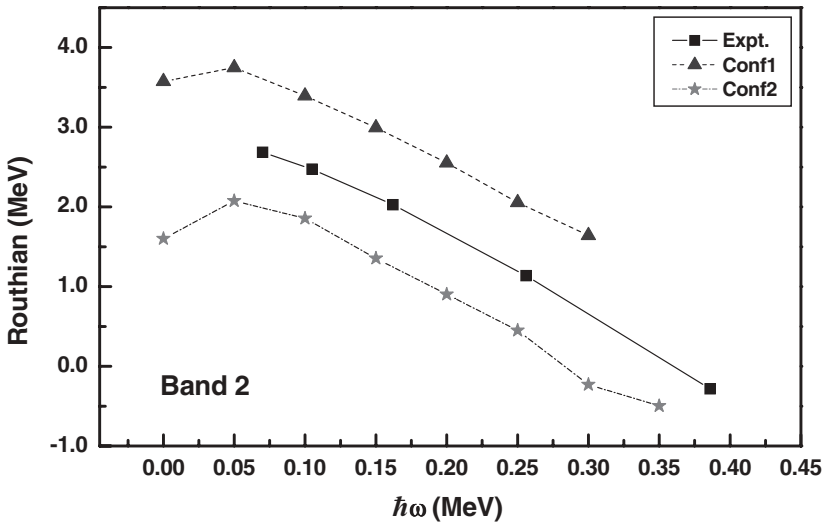

FIG. 9. Experimental Routhian for band 2 plotted as a function of the rotational frequency and compared with the theoretical Routhians corresponding to the two configurations Conf1 and Conf2. See text for details.

positive-parity band 2. Considering the systematics for $N = 79$ odd-A isotones [38] along with the present theoretical results with different three-qp configurations, we conjecture that the possible configuration for the low-lying states of band 2 of ^{137}Ce, including the $\frac{19}{2}\hbar$ bandhead, would be $\nu h^2_{\frac{11}{2}} \otimes \nu s_{\frac{1}{2}}$ (i.e., Conf2) and for the states above $\frac{25}{2}\hbar$, a configuration of $\pi g_{\frac{7}{2}} h_{\frac{11}{2}} \otimes \nu h_{\frac{11}{2}}$ (i.e., Conf1) would be effective.

C. Band 6

This band is developed on the 5379.1-keV $\frac{33}{2}^+$ state and extends to the 7660.3-keV ($\frac{43}{2}^+$) level. The γ rays assigned to this band are dominantly $M1$ in nature with small $E2$ admixtures. No crossover $E2$ transition was seen. Zhu *et al.* [23] assigned a negative parity and oblate shape for this band and suggested a configuration of $\pi g_{\frac{7}{2}} h_{\frac{11}{2}} \otimes \nu h^2_{\frac{11}{2}} s_{\frac{1}{2}}$ with $\gamma = -60^\circ$, based on a systematic comparison with the oblate bands (i.e., bands 1, 3, and 5 in ^{135}Ce [10]). A comparison of the experimental alignment of band 6 from the present work with that of band 5 in ^{135}Ce and band 5 in ^{136}Ce [13] (cf. Fig. 5) clearly shows a similar trend, though the value of the alignment is ∼2 units less than that for band 5 in ^{135}Ce. It is conjectured that the observed reduced alignment in band 6 of ^{137}Ce may be due to the involvement of fewer high-Ω $h_{\frac{11}{2}}$ orbitals in the bandhead configuration, compared to that in band 5 of ^{135}Ce. The alignment plot for band 6 (cf. Fig. 5) is more or less flat for all ω, indicating that there is little extra alignment with increase in frequency. It is also observed that the alignment values are similar to that of band 5 in ^{136}Ce [13], which has a four-qp configuration: $\pi g_{\frac{7}{2}} h_{\frac{11}{2}} \otimes \nu h_{\frac{11}{2}} g_{\frac{7}{2}}$ with $\gamma \sim 28^\circ$. The $J^{(1)}$ and $J^{(2)}$ values for band 6 have been plotted with rotational frequency (ω) in Figs. 7 and 8, respectively, along with that for band 2 of ^{137}Ce. The relatively steeper fall of $J^{(1)}$ and a rather flat nature and low value of $J^{(2)}$ indicate that the band is likely to have a triaxial deformation. The $J^{(1)}$ and $J^{(2)}$ values have been compared with those of band 5 in ^{135}Ce [10] and show a similar trend. We have calculated the experimental Routhian values for band 6, considering the calculated value of $\langle K \rangle \approx 15.5$, as discussed in the first paragraph of this section, and plotted these values with respect to the angular frequency ω in Fig. 10. The TRS calculation

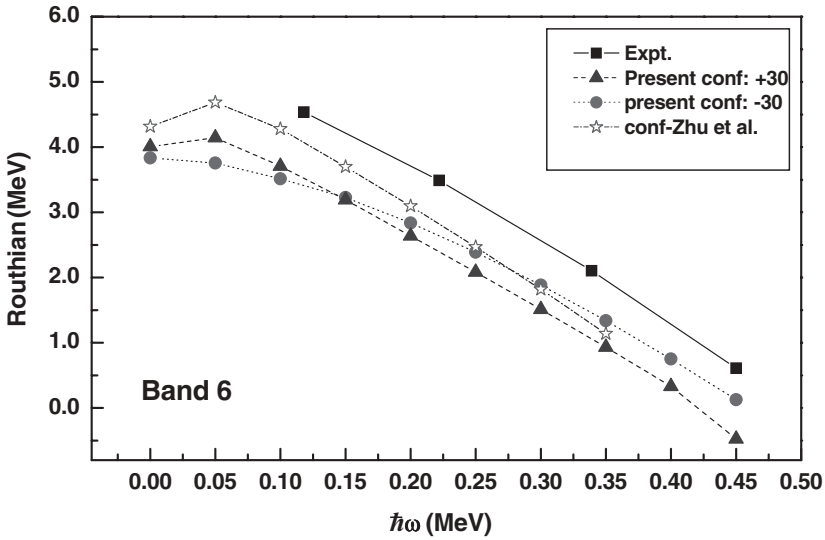

FIG. 10. Experimental Routhian for band 6 plotted as a function of the rotational frequency and compared with the theoretical Routhians. See text for details.

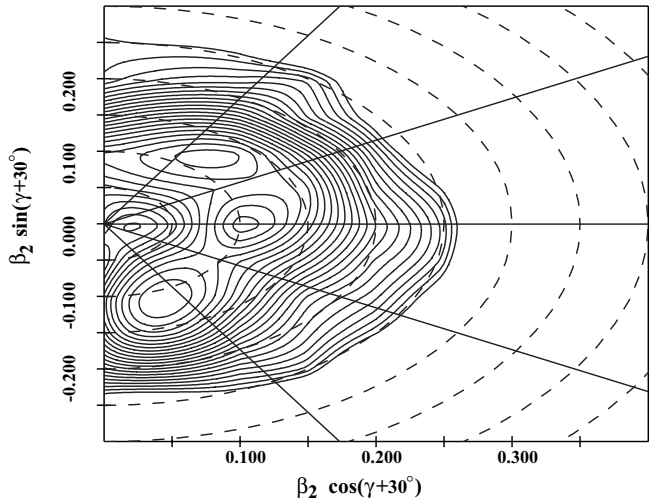

FIG. 11. The potential energy surface plotted in the β-γ plane for the proposed configuration of band 6 at the bandhead frequency $\approx$0.1 MeV.

[24–26] has been performed for this band by considering different five-qp configurations and the results have been compared with the experimental values. The configuration $\pi(+,+1/2)(-,+1/2)\nu(+,+1/2)^2(-,+1/2)$ gives rise to a positive-parity band with two consistent deformation minima at $\gamma = \pm 30^\circ$, present throughout the range of ω values considered (cf. Fig. 11). The Routhian plots for the two minima cross each other at a ω value very close to the bandhead frequency. It has been observed that the Routhian for the $+30^\circ$ minima matches well with the experimental plot, as shown in Fig. 10. The other predicted band with $\gamma = -30^\circ$, most likely, remains unobserved. We have calculated the Routhians for the configuration proposed by Zhu *et al.* [23] also [i.e., for $\pi(+,+1/2)(-,+1/2)\nu(+,+1/2)(-,+1/2)^2$], which gives rise to a negative-parity band with an oblate minima. This configuration was conjectured by Zhu *et al.* from a comparison of the kinematic and dynamic moments of inertia ($J^{(1)}$ and $J^{(2)}$) values with those of band 5 in ^{135}Ce [10]. The Routhian plot for this configuration has been included in Fig. 10 for comparison. This comparison favors the former configuration, given by us, supporting our assignment of positive parity to band 6 with $\beta_2 = 0.14$ and $\gamma = +30^\circ$. It is therefore concluded from this discussion that band 6 in ^{137}Ce has been formed by the addition of an extra $g_{\frac{7}{2}}$ neutron quasiparticle to the configuration of band 5 in the ^{136}Ce nucleus [13]. The addition of a single $\nu g_{\frac{7}{2}}$ quasiparticle has not changed the alignment much and has not contributed to the deformation. The five-qp configuration proposed for this band is, therefore, $\pi(+,+1/2)(-,+1/2)\nu(+,+1/2)^2(-,+1/2)$, that is, $\pi g_{\frac{7}{2}} h_{\frac{11}{2}} \otimes \nu h_{\frac{11}{2}} g^2_{\frac{7}{2}}$, which matches well with the experimental Routhian.

D. Bands 3, 4, and 5

Besides bands 1, 2, and 6, we have identified two more bandlike sequences (band 3 and band 4) and a weak cascade of two transitions, labeled as band 5, above the 3724.7-keV ($\frac{25}{2}^+$) state. This band connects band 3 by the 320.1-keV $M1$ transition.

Band 3, with positive parity, is developed on the 3128.4-keV $\frac{21}{2}^+$ level and connected to band 1 by the 937.2-keV $E1$ transition. This band extends to 3985.3 keV and connects to band 4 by the 269.7-keV $E2$ transition. We propose a three-qp configuration of $\pi g_{\frac{7}{2}} d_{\frac{5}{2}} \otimes \nu s_{\frac{1}{2}}$ to band 3 and a five-qp configuration of $\pi g_{\frac{7}{2}} d_{\frac{5}{2}} h^2_{\frac{11}{2}} \otimes \nu s_{\frac{1}{2}}$ to band 4. A possible band crossing between these two bands is conjectured to arise from a proton pair excitation to the $h_{\frac{11}{2}}$ orbital. Recently, a similar band crossing has been suggested by Kumar *et al.* [38] in the $N = 79$ ^{139}Nd nucleus. To confirm the possible band crossing and the structure of the weak-side bands, it is necessary to study this nucleus to the higher angular momentum states by using a heavier projectile.

V. CONCLUSION

The high spin states of ^{137}Ce have been investigated by using a modest Clover Ge array. Two prominent bandlike sequences (band 2 and band 6) have been established, in addition to the well-known negative-parity ground-state band (band 1). The properties of these bands have been examined by performing a total Routhian surface calculation and are found to be similar to the other collective bands, which are systematically observed in $N \geqslant 77$ nuclei in this mass region, having three- and five-qp configurations, respectively. A side-by-side comparison of the level schemes of ^{137}Ce and ^{135,136}Ce reveals that many of the band structures in ^{137}Ce might have been missed in the present reaction because of their low intensity and the limited efficiency of the array. This is further supported from the TRS results also, in which we see many stable minima for different multi-quasiparticle configurations. It would, therefore, be worthwhile to reinvestigate the high-spin structure of this nucleus by using a larger array and a suitable target-projectile combination, keeping in view the possibility of observing highly deformed triaxial bands as have been observed in ^{139}Nd [18].

ACKNOWLEDGMENTS

The authors thank the members of the INGA Collaboration who were responsible for setting up the early implementation of the Clover Array at IUAC, New Delhi. They are grateful to the operating staff of the 15UD Pelletron for their helpful co-operation and the staff of the Target Laboratory of VECC, Kolkata, for their help in preparing the enriched target. T.B. would like to express her sincere thanks to Dr. Gopal Mukherjee for meaningful academic discussion on TRS calculations. The Teacher Fellowship supported by the University Grants Commission (UGC), Government of India, to S.C. is gratefully acknowledged.

[1] D. B. Fossan *et al*., Nucl. Phys. **A520**, 241c (1990).
[2] M. A Rizzutto *et al*., Nucl. Phys. **A569**, 547 (1994).
[3] I. Ragnarsson *et al*., Nucl. Phys. **A233**, 329 (1974).
[4] Y. S. Chen, S. Frauendorf, and G. A. Leander, Phys. Rev. C **28**, 2437 (1983).
[5] B. D. Kern *et al*., Phys. Rev. C **36**, 1514 (1987).
[6] E. S. Paul *et al*., Phys. Rev. Lett. **58**, 984 (1987).
[7] E. S. Paul, D. B. Fossan, Y. Liang, R. Ma, and N. Xu, Phys. Rev. C **40**, 1255 (1989).
[8] R. Wyss *et al*., Phys. Lett. **B215**, 211 (1988).
[9] S. Frauendorf and F. R. May, Phys. Lett. **B125**, 245 (1983).
[10] R. Ma *et al*., Phys. Rev. C **41**, 2624 (1990).
[11] E. S. Paul *et al*., Phys. Rev. C **41**, 1576 (1990).
[12] S. Lakshmi *et al*., Phys. Rev. C **66**, 041303(R) (2002).
[13] S. Lakshmi *et al*., Nucl. Phys. **A761**, 1 (2005).
[14] T. Bhattacharjee *et al*., Nucl. Phys. **A750**, 199 (2005).
[15] G. Gangopadhyay *et al*., Eur. Phys. J. A **24**, 173 (2005).
[16] M. L. Li *et al*., Phys. Rev. C **75**, 034304 (2007).
[17] C. M. Petrache *et al*., Phys. Lett. **B373**, 275 (1996).
[18] C. M. Petrache *et al*., Phys. Rev. C **61**, 011305(R) (1999).
[19] J. Ludziejewski *et al*., Z. Phys. A **281**, 287 (1977).
[20] M. Müller-Veggian *et al*., Nucl. Phys. **A304**, 1 (1978).
[21] M. Kortelahti *et al*., Phys. Scr. **27**, 166 (1983).
[22] J. K. Tuli, Nucl. Data Sheets **72**, 355 (1994).
[23] S. J. Zhu *et al*., Phys. Rev. C **62**, 044310 (2000); B. Browne and J. K. Tuli, Nucl. Data Sheets **108**, 2173 (2007).
[24] P. Ring and P. Schuck, *The Nuclear Many-Body Problem* (Springer-Verlag, Berlin, 2004), p. 126.
[25] W. Nazarewicz, M. A. Riley, and J. D. Garrett, Nucl. Phys. **A512**, 61 (1990).
[26] W. Nazarewicz *et al*., Nucl. Phys. **A435**, 397 (1985).
[27] A. Gavron, Phys. Rev. C **21**, 230 (1980).
[28] R. K. Bhowmik *et al*., in *Proceedings of the DAE Symposium on Nuclear Physics* **B44**, 422 (2001).
[29] G. Duchène *et al*., Nucl. Instrum. Methods Phys. Res. A **432**, 90 (1999).
[30] R. K. Bhowmik (private communication, 2002).
[31] A. A. Sonzogni, Nucl. Data Sheets **98**, 515 (2003).
[32] S. Chanda *et al*., in *Proceedings of the DAE-BRNS Symposium on Nuclear Physics* **B46**, 114 (2003).
[33] A. Krämer-Flecken *et al*., Nucl. Instrum. Methods Phys. Res. A **275**, 333 (1989).
[34] P. M. Jones *et al*., Nucl. Instrum. Methods Phys. Res. A **362**, 556 (1995).
[35] Ch. Droste *et al*., Nucl. Instrum. Methods Phys. Res. A **378**, 518 (1996).
[36] K. Starosta *et al*., Nucl. Instrum. Methods Phys. Res. A **423**, 16 (1999).
[37] R. Bengtsson and S. Frauendorf, Nucl. Phys. **A327**, 139 (1979).
[38] S. Kumar *et al*., Phys. Rev. C **76**, 014306 (2007).